Proceedings of the 9th International Conference on Fluid Flow, Heat and Mass Transfer (FFHMT'22)
Niagara Falls, Canada – June 08-10, 2022
Paper No. 213
DOI: 10.11159/ffhmt22.213

Enhancement of the Parallel and Series Mode of the Ultrasonic Atomizer on the Ammonia-Water Falling Film Absorber

Runfa Zhou[1], Minqi Wang[1], Shuhong Li[1*]
[1] School of Energy and Environment, Southeast University,
Nanjing, Jiangsu, China, 210094.
Runfa Zhou, 230198437@seu.edu.cn; Minqi Wang, 220190520@seu.edu.cn
[*]Corresponding author: Shuhong Li, School of Energy and Environment, Southeast University, Nanjing, Jiangsu, China, 210094, equart@seu.edu.cn

Abstract: Falling film absorber is widely used in the ammonia-water absorption refrigeration system, and the mass transfer area can be enlarged by the atomization device to overcome the shortages of low system energy efficiency and large system size. Ultrasonic atomizer can produced micron size droplets, so the liquid-vapor contact area can be further enlarged. Considering the large flight resistance of the small size droplets, the ultrasonic atomizer devices are located at the top of the absorber, and two installation strategies (i.e., parallel and series) are proposed. To analyze the improvement of the novel absorber with the installation of the atomizer, a mathematical model to describe the mass and heat transfer of the novel absorber is established. The model is verified by the reported data of literature, and the enhancement effects of the parallel and series installation strategies of the atomizer are discussed by the validated model. In the condition of this paper, compared with traditional falling film absorber, the ammonia absorbed rate is increased by 22.5% for the parallel installation strategy and 17% for the series installation strategy. Compared with the improvement of the cooling capacity, the energy consumption of the atomizer is worth.

Keywords: Absorption refrigeration system, Falling film absorber, ultrasonic atomizer, ammonia absorbed rate

NOMENCLATURE

c_p	specific heat [J/(kg·℃)]
C	concentration [mol/m^3]
d	diameter [m]
D	diffusion coefficient [m^2/s]
f_d	drag coefficient [dimensionless]
f	force [N]
F	volumetric force [N/m^3]
g	gravitational acceleration [m/s^2]
h	specific enthalpy [J/kg]
k	mass transfer coefficient [m/s]
L	length [m]
m	mass [kg]
$\dot{m}$	mass flow rate [kg/s]
n	number of droplets [dimensionless]
n	normal vector [m]
M_a	molecular weight of ammonia [kg/mol]
Re	Reynolds number [dimensionless]
$\dot{S}_m$	source term of mass [kg/(m^3 s)]
s_m	ammonia absorbed rate of single droplets [kg/s]
$\dot{S}_T$	source term of energy [W/m^3]
s_T	heat transfer of single droplets [W]
t	time [s]
T	temperature [℃]
U	heat transfer coefficient [W/(m^2·℃)]
v	velocity [m/s]

Greeks

α	volume fraction [dimensionless]
β	atomization ratio [dimensionless]
δ	thickness of the falling film [m]
ΔV	volume of the calculation elements [m^3]
ρ	density [kg/m^3]
λ	thermal conductivity [W/(m·℃)]
μ	viscosity [Pa s]

Subscripts

b	tube wall
eff	effective
d	drag
f	falling film solution
L	lift
nt	nominal
p	droplets
s	droplets surface
v	vapor
w	water

Introduction

The energy crisis caused by the increase of energy consumption with the development of the economy is widely concerned. Compared with polluting and non-renewable fossil fuel, clean and renewable energy such as geothermal energy, solar energy, industrial waste heat, etc, has wide prospects [1, 2]. The absorption refrigeration system (ARS) can realize the effective utilization of above low-grade energy sources [3, 4]. The absorbent and refrigerant of ammonia water are environment friendly and low-cost, and it is concerned in these decades [5, 6]. However, the limitation of the enormous size and low energy efficiency restricts the application of the ammonia water absorption refrigeration system [7].

Absorber is the fundamental equipment of the ARS, and its mass transfer area occupies more than 50% of the total system [8, 9]. Meanwhile, the mass fraction difference of the inlet and outlet determines the mass flow rate of absorbent in the system, which influences the heat load of the generator and absorber. The heat transfer resistance leads to the temperature difference of coolant and solution, and the mass transfer resistance results in the solution at the outlet being unsaturated [10, 11]. Therefore, enhancing heat and mass transfer to decrease the temperature difference between the solution and coolant, and the mass fraction difference of solution between the outlet state and saturated sated will improve the outlet solution mass fraction. The increase solution mass fraction at the absorber outlet can decrease the heat load of the generator and absorber, and improve the energy efficiency of the ARS [4, 12].

Liquid atomization is widely applied on on many industrial processes to enhance mass and heat transfer, such as drying [13], internal combustion engines [14, 15], SO2 and CO2 capture [16-19]. Li et al. [17] used air-blast spray technology to atomize the aqueous solution of sodium hydroxide in the CO2 capture device and proved that the volumetric mass transfer coefficient has a great improvement after the atomization. Kuntz [20, 21] compared the volumetric mass transfer coefficient of CO2 captured by MEA in the spray absorber and packed absorber. The volumetric mass transfer coefficient of spray absorber is 2-7 times higher than packed absorber. The solution atomization is utilized in the fermentation process of synthesizer by Sathish et al. [22], and the volume mass transfer coefficient increases by a hundred times.

Converting the solution into small size droplets by atomization technology, the vapor-liquid contact area can be significantly enlarged. The contact area is inversely proportional to the droplet diameter. Compared with air-blast, the ultrasonic atomizer can obtain droplets in the micron grade without the driven pressure [23, 24]. By installing the ultrasonic atomizer, Yang et al. [13, 25] atomized the desiccant to absorb water vapor. The consumption of the dehumidifier is reduced by 45%. Li et al. [26] proposed a desiccant regeneration system with the method of ultrasonic atomization and the regeneration temperature is decreased by 3.1-6.6℃.

There are two installation strategies of the atomizer: parallel or series mode. In the parallel mode, the solution is atomized before the falling film process. In the series mode, the solution is atomized after the falling film process. In this paper, a novel falling film absorber installed with ultrasonic atomizer is proposed, and the parallel or series modes of the atomizers are compared. The atomizer is placed at the top of the falling film tube. A mathematical model describing the absorption process of novel absorber is established. The atomization absorption and falling film absorption are coupled by the heat and mass transfer at the phase interface in the model. The model is validated by the reported data in the reference [8, 27, 28]. The improvement of two installation strategies on absorption effect is calculated by the verified model. Furthermore, the influence of the energy consumption of the atomization process is discussed. The present work is the starting point prior to further product design, manufacture and test.

1. Absorber Description

1.1. Novel absorber

The traditional falling film mode without the atomizer is named Mode A. The weak solution flows into the solution distribution plate (SDP) from the absorber inlet. After overflowing from the SDP, the solution forms the falling film and attaches to the falling film tube (FFT) under the action of surface tension and gravity. The ammonia vapor is fed into the absorber from the vapor inlet. Before the solution falls into the solution collecting tank (SCT), the vapor is absorbed by the falling solution. The cooling water flows in the inverse direction of falling film to cool the solution.

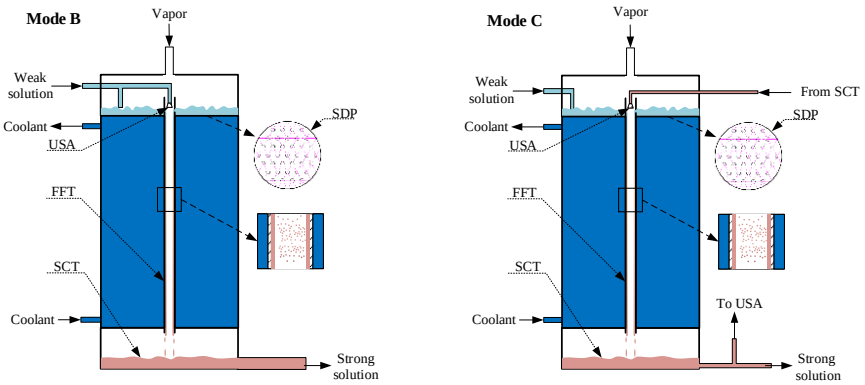

Fig. 1 The schematic diagram of falling film absorber with atomizer

Based on the difference of the atomizer installation strategies, the parallel and serial modes are named Mode B and Mode C, respectively. The absorbers of Mode B and Mode C are shown in Fig. 1(a) and Fig. 1(b), respectively. In Mode B, a part of the inlet solution is atomized to droplets, and the other solution continues the falling film process. In Mode C, a part of the solution of the SCT flows out of the absorber, and the other part is pumped to the ultrasonic atomizer (USA).

After installing the USA, the atomization droplets disperse in the vapor zone and absorb ammonia. The falling film absorption and atomization absorption process are carried out simultaneously in the absorber. After the absorption process, the falling film solution is mixed with the droplets at the SCT.

The structure parameters are listed in Table 1, and the novel falling film absorber is installed in the ARS shown in Fig. 2. The system operation parameters are also listed in Table 1. In Mode C, the solution pump (SP2) is used to pump the solution from SCT to the USA, but in Mode A and Mode B, it is switched off.

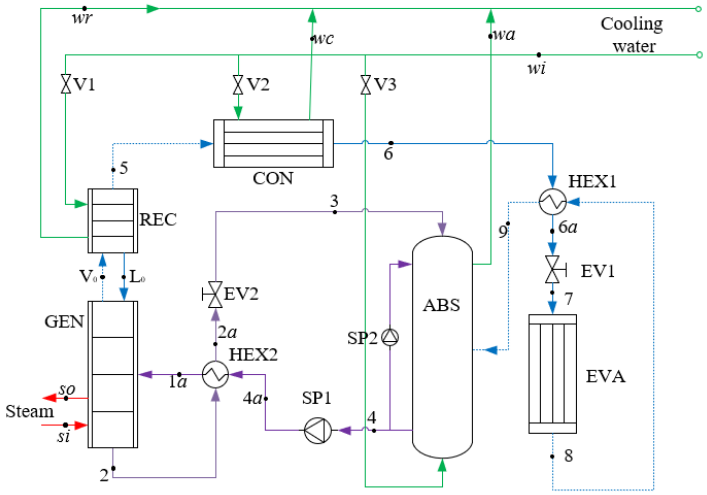

Fig. 2 The absorption refrigeration system with the novel falling film absorber

(GEN: generator. REC: rectifier. CON: condenser. HEX1, HEX2: heat exchanger. EV1, EV2: expansion valve. EVA: evaporator. ABS: absorber. SP1, SP2: solution pump. V1~V3: valve.)

Table 1 Refrigeration system operation parameters and absorber structure parameters

Parameters	Unit	Value
Falling film tubes type		Φ25.4*1.2 ANSI 304
Numbers		37
Length:	m	1

Arrangement		staggered arrangement
Longitudinal tube pitch	mm	63.5
Transverse tube pitch	mm	55
Altitude difference between the USA and SCT	m	1.2

1.2. Ultrasonic atomizer

The ceramic slice of USA can be installed inside the FFT owing to a tiny size. The droplets will be generated at the phase interface after immersing the ceramic slice into the solution. According to reference [25], when the diameter and the generated rate of droplets are 50 μm and 50 kg/h, the atomizer power is 50 W. It is assumed that the energy consumption of atomizer is positively proportional to generated rate and inversely proportional to the diameter of the droplets. The energy consumption of the atomizer in this paper is calculated by this principle.

Defined as the ratio of droplets generating and inlet solution mass flow rate, the atomization ratio is expressed as

$$\beta = \frac{\dot{m}_p}{\dot{m}_3} \qquad (1)$$

Remarkably, the energy consumption of absorption process in Mode B is the atomizer power, but the work of solution pump needs to be considered in Mode C. Neglect the energy loss, the solution pump work is equal to the difference of gravitational potential energy between the absorber outlet and the atomizer.

2. Mathematical Model

2.1. Source terms

Considering the symmetry of the absorption process, the tangential velocity of solution and vapor side is negligible. The thickness of the solution film is small and the solution flows at a low velocity. The vapor zone is combined with ammonia vapor and unsaturated droplets. The low volume fraction of droplets means that the DPM (discrete particle model) can be implemented to describe the interactions of droplets and vapor [30]. The ammonia vapor is the continuous phase, and the interactions of droplets and vapor conclude the mass, momentum and energy exchange, and the source terms of the governing equations is the volume average value of these interactions.

$$\mathbf{F} = -\frac{1}{\Delta V}\sum_{i=1}^{n}\left(\mathbf{f}_{\mathrm{L},i} + \mathbf{f}_{\mathrm{d},i}\right) \quad (2)$$

$$\dot{S}_{\mathrm{m}} = -\frac{1}{\Delta V}\sum_{i=1}^{n} s_{\mathrm{m},i} \qquad (3)$$

$$\dot{S}_{\mathrm{T}} = -\frac{1}{\Delta V}\sum_{i=1}^{n}\left(s_{\mathrm{T},i}\right) \qquad (4)$$

The movement of single droplet is affected by gravity, lift and drag. The dynamical equation of droplet is

$$m_{\mathrm{p}}\frac{d\mathbf{v}_{\mathrm{p}}}{dt} = m_{\mathrm{p}}\mathbf{g} + \mathbf{f}_{\mathrm{L}} + \mathbf{f}_{\mathrm{d}} \quad (5)$$

The lift is mainly caused by the buoyancy, and the drag can be expressed as:

$$\mathbf{f}_{\mathrm{d}} = \frac{1}{2} f_{\mathrm{d}} \rho_{\mathrm{v}} \pi d_{\mathrm{p}}^2 \left|\mathbf{v}_{\mathrm{v}} - \mathbf{v}_{\mathrm{p}}\right|\left(\mathbf{v}_{\mathrm{v}} - \mathbf{v}_{\mathrm{p}}\right) \qquad (6)$$

where the drag coefficient is the function of Reynolds number [31]. The mass and heat transfer can be expressed as:

$$s_m = M_{\mathrm{a}} k_s \pi d_{\mathrm{p}}^2 (C_{\mathrm{v}} - C_{\mathrm{p}}) \qquad (7)$$

$$s_T = U_s \pi d_{\mathrm{p}}^2 \left(T_{\mathrm{v}} - T_{\mathrm{p}}\right) + s_{\mathrm{m}}\left(h_{\mathrm{v}} - h_{\mathrm{p}}\right) \qquad (8)$$

For the mass and heat transfer between the spherical droplet and vapor, the correlations of transfer coefficient are fully reported, and the correlation of Ranz and Marshall [31] is used in this paper.

2.2. Phase interface

The heat and mass exchange between vapor and falling film solution side is through the phase interface. Based on the mass conservation, the mass exchange through the phase interface can be expressed as

$$-D_{\mathrm{v}}\frac{\partial C_{\mathrm{v}}}{\partial \mathbf{n}}+\alpha_{\mathrm{p}}\rho_{\mathrm{p}}\mathbf{v}_{\mathrm{p}}\mathbf{n}=-D_{\mathrm{f}}\frac{\partial C_{\mathrm{f}}}{\partial \mathbf{n}} \quad (9)$$

where the first term of the left side is caused by diffusion, and the second term is caused by the droplets being captured by the falling film solution. Similarly, the energy conservation can be expressed as

$$-\lambda_{\mathrm{v}}\frac{\partial T_{\mathrm{v}}}{\partial \mathbf{n}}-D_{\mathrm{v}}\frac{\partial C_{\mathrm{v}}}{\partial \mathbf{n}}\left(h_{\mathrm{v}}-h_{\mathrm{f}}\right)+\alpha_{\mathrm{p}}\rho_{\mathrm{p}}h_{\mathrm{p}}\mathbf{v}_{\mathrm{p}}\mathbf{n}=-D_{\mathrm{f}}\frac{\partial C_{\mathrm{f}}}{\partial \mathbf{n}} \quad (10)$$

The assumption of free liquid level is satisfied at the phase interface, so the velocity gradient is zero. The location of phase interface is obtained by Geselleschaft's correlation [32].

2.3. Boundary conditions

The structure parameters and operation conditions of FFT are listed in Table 1 and Table 2, respectively. The selection of inlet conditions is based on an ideal ARS with cooling capacity of 2.9 kW. The condensing temperature and evaporation temperature and generation temperature are 30 ℃ and -15 ℃ and 125 ℃, respectively. The ammonia at the outlet of the condenser and evaporator is saturated. After flowing out of the evaporator, the ammonia vapor is overheated to the surrounding temperature (20 ℃).

The heat transfer between the solution and cooling water satisfies the third boundary condition

$$-\lambda_{\mathrm{f}}\frac{\partial T_{\mathrm{f}}}{\partial \mathbf{n}}=U_{\mathrm{b}}(T_{\mathrm{w}}-T_{\mathrm{f}}) \quad (11)$$

where heat transfer coefficient (Ub) is calculated by the thermal resistance of cooling water and tube wall. The material of FFT is stainless steel of ANSI 304. The convection heat transfer coefficient is calculated by Dittus Boelter's correlation [31]. The temperature of cooling water can be calculated by the energy conservation equation of the solution side

$$\dot{m}_{\mathrm{w}}c_{p,w}\frac{dT_{\mathrm{w}}}{dL}=U_{\mathrm{b}}\pi d_{\mathrm{nt}}(T_{\mathrm{w}}-T_{\mathrm{f}}) \quad (12)$$

where the d_{nt} is the nominal diameter of the FFT.

Table 2 The operation condition of absorber

Parameters	Unit	Value
Inlet temperature of cooling water	℃	20
Mass flow rate of cooling water of each tube	kg/h	231
Mass flow rate of dilute solution of each tube	kg/h	1.61
Inlet mass fraction of dilute solution		0.258
Inlet temperature of dilute solution	℃	40
Inlet temperature of ammonia vapor	℃	20
Pressure of absorber	MPa	0.3
Droplets diameter	μm	50
Atomization ratio of Case B		0.5
Atomization ratio of Case C		0.5

3. Model Validation

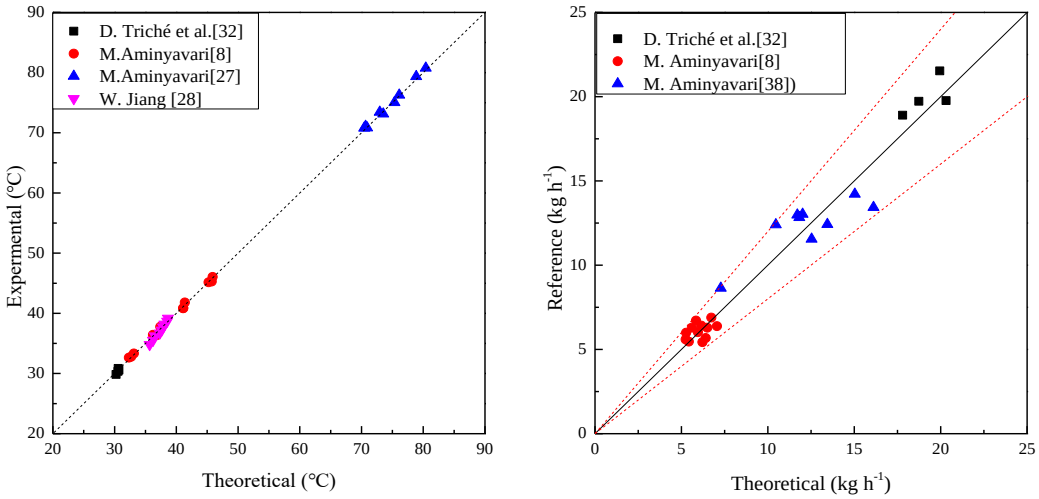

(a) (b)

Fig. 3 Theoretical results versus reference results: (a) outlet solution temperature (b) ammonia absorber rate

To ensure the correction of theoretical analysis, the experimental measurements in the reference of falling film absorber are utilized to verify the model. With the inlet conditions reported in the public reference, the outlet cooling water temperature and ammonia absorbed rate is calculated by the established model. The comparison of the theoretical calculated and reference results is shown in Fig. 3. Jiang et al [28] did not report the ammonia absorbed rate, and the outlet mass fraction of the solution is calculated as saturated, so the comparison is not listed in Fig. 3. Aminyavari et al [27] has higher absorption pressure and cooling temperature (1.8 MPa, 70 ℃), which causes the larger relative error at some point, but the error can be accepted. The maximum outlet temperature error of cooling water and the maximum relative error of ammonia absorbed rate are 0.5 ℃ and 20%, respectively. Therefore, the theoretical results match well with the experimental data of the reference.

4. Results And Discussion

4.1. Mode A

As the referring benchmark, the mass and heat transfer in the ammonia absorption process of Mode A is calculated, and the boundary condition is listed in Table 1 and Table 2. Remarkably, the mass flux and heat flux are defined as the mass transfer and the heat transfer for the per unit area of FFT, so the enhancement effect of the area enlarged by droplets on heat and mass transfer can be characterized. For the ideal absorber with infinite heat and mass transfer area, the temperature and mass fraction of the outlet solution is 20 ℃ and 0.4845 based on the inlet conditions listed in Table 2.

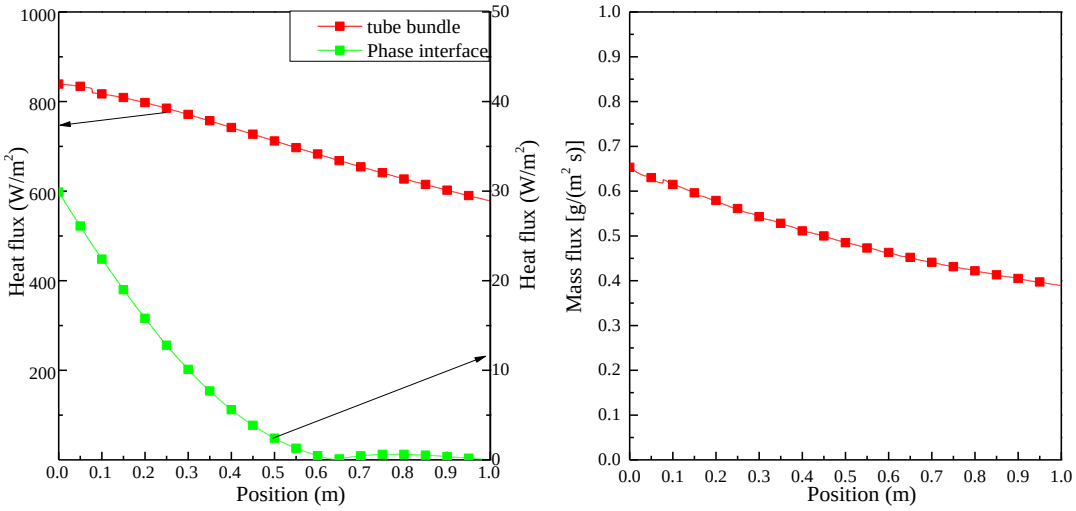

(a) (b)

Fig. 4 The mass and heat transfer characteristics of Mode A

The heat and mass transfer characteristics of Mode A, such as the distribution of heat flux and mass flux, are shown in Fig. 4. The inlet solution is cooled by the cooling water so the temperature decreases with the falling film process. The vapor temperature at the inlet is lower than the solution, and the heat transfer between the solution and the vapor results in the temperature increasing at the start of the absorption process and then decreasing. At the position of x =0.636 m, the vapor temperature reaches the maximum value of 28.3 ℃. The outlet temperatures of the cooling water and the solution are 20.3 ℃ and 27.2 ℃, respectively.The solution mass fraction is 0.3327 at the outlet of Mode A. However, for the solution temperature at the outlet, the mass fraction is 0.4386 if the solution is saturated. Therefore, the outlet solution mass fraction has a sizable improvement potential. Besides that, compared with the ideal absorber, the outlet temperature of Mode A can also be further decreased by enhancing the cooling effect.

The ammonia absorbed rate of the single FFT is 0.0547 g/s, and the average mass flux of the FFT is 0.498 g/(m^2 s). The heat transfer rate between the cooling water and the solution for the single FFT is 78.2 W, and the average heat flux is 712 W/m^2. Moreover, the heat transfer between the ammonia vapor and the solution for the single FFT is 0.78 W, and the average heat flux is 7.26 W/m^2.

4.2. Mode B

For the atomization parameters listed in Table 2, the atomization ratio is 0.5 and the initial diameter is 50 μm. The solution atomized rate is 0.805 kg/h, the energy consumption of atomizer for single FFT is 0.805 W based on the calculation method mentioned in section 2.1 of this paper. The heat and mass transfer characteristics of Mode B are shown in (a) (b)

Fig. 5. The outlet temperature of cooling water and solution is 20.26 ℃ and 24.28 ℃. Compared with Mode A, the mass flow rate of falling film solution is decreased, so the solution temperature after falling film process of Mode B is decreased. A lower solution temperature means a larger ammonia absorbed rate, so the mass fraction after falling film process of Mode B is 0.3651.

The mass and heat transfer rate increases with the decreasing of droplets diameter, and the heat generated increases with the ammonia absorbed. Therefore, the temperature of droplets rises rapidly at the top of the absorber because of the high mass transfer rate and ineffective cooling in the atomization absorption process. Because the high temperature inhibits the ammonia absorbed in atomization absorption process, the mass transfer rate decreases, and the heat generated also decreases. The small size of droplets brings effective heat exchange between the droplets and the vapor, so the vapor temperature is close to the droplets temperature at the whole absorption process. The vapor is heated by the atomization

absorption process at the top of the absorber. After the weakened of atomization absorption, the vapor is gradually cooled by the falling film solution, so the temperature of vapor and droplets is also decreased. At the bottom of the absorber, the temperature and mass fraction of droplets are 47.9 ℃ and 0.3315, respectively.

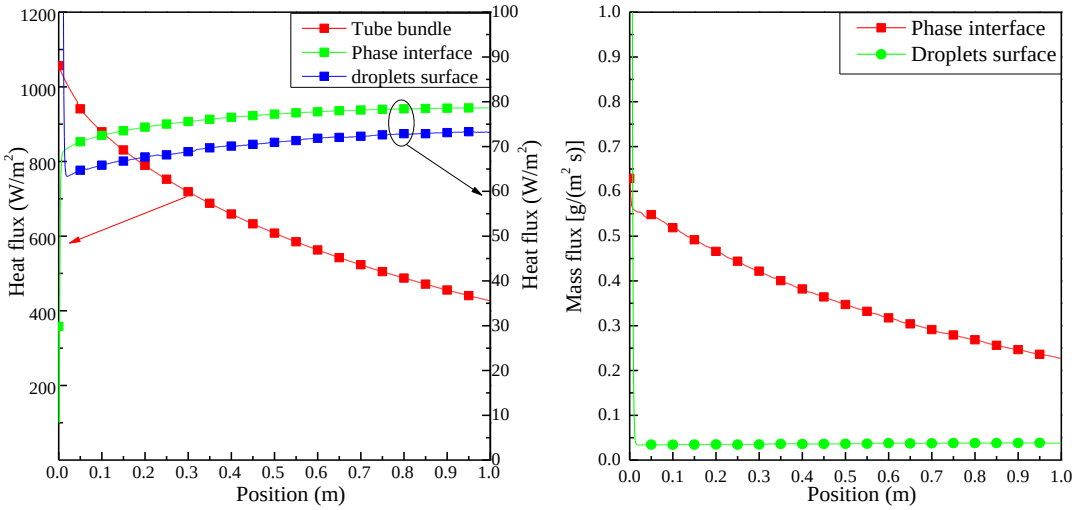

(a) (b)

Fig. 5 The mass and heat transfer characteristics of Mode B

The droplets and falling film solution are mixed at the SCT and flows out of the absorber. The temperature and mass fraction of the solution at the outlet are 35.8 ℃ and 0.3488, respectively. Compared with Mode A, both of the outlet solution temperature and mass fraction in Mode B are increased.

In Mode B, the ammonia absorbed rate of the single FFT is 0.0402 g/s for the falling film absorption, and it is 0.0269 g/s for atomization absorption. Correspondingly, the average mass flux of falling film interface and droplets interface is 0.3654 g/m^2 s and 0.2449 g/m^2 s. The total ammonia absorbed rate is 0.0670 g/s, which is increased by 22.5% compared to Mode A. Furthermore, the cooling load of Mode B is 70.40 W, and the heat flux through the FFT is 640 W/m^2. The cooling effect is reduced by 10.5%, which is caused by the decreasing of the falling film solution thickness. Meanwhile, the heat transfer through the phase interface of the falling film solution increases with the vapor temperature. The total heat transfer rate of the single FFT between the vapor and falling film solution is 8.36 W, and the average heat flux is 76.11 W/m^2.

4.3. Mode C

Compared with Mode B, Mode C has extra energy consumption of the solution pump. For the atomization ratio and droplets diameter listed in Table 2, the work of solution pump is 0.1 W, so the total energy consumption of absorber in Mode C is 29.88 W. The mass and heat transfer characteristics are shown in (a) (b)

Fig. 6. The outlet temperature of cooling water and falling film solution is 20.3 ℃ and 27.35 ℃, respectively. Compared with Mode A, the falling film solution is heated because of the heat generated in the atomization absorption process. Therefore, the falling film absorption is inhibited, and the solution mass fraction after falling film is 0.3289 and slightly lower than model A. Moreover, compared with Mode B, the initial solution of atomization droplets is higher, so the ammonia absorbed rate of atomization absorption process in Mode C is lower. Similarly, the heat generated in atomization absorption process is lower than Mode B. The temperature and mass fraction of the droplets after the atomization absorption process is 38.35 ℃ and 0.3787, respectively. The droplets fall into the SCT and mix with the falling film solution, and the temperature and the mass fraction at the absorber outlet are 30.88 ℃ and 0.3449, respectively.

Meanwhile, the total ammonia absorbed rate in Mode C is 0.0640 g/s. Compared with Mode A, the ammonia absorbed rate is increased by 17%. The ammonia absorbed rate in the falling film absorption process is 0.0518 g/s, and in

the atomization absorption process is 0.0122 g/s. Correspondingly, the average mass flux is 0.4718 g/m^{2}s and 0.1106 g/m^{2}s, respectively. Compared with Mode A, the heat load of cooling water is increased by 2%, because the droplets increase the temperature of vapor. The heat transfer rate between cooling water and falling film solution is 79.83 W, and the average heat flux is 726 W/m^2. The higher vapor temperature also increases the heat transfer rate between the vapor and falling film solution, and the heat transfer rate is 3.51 W, so the average heat flux is 31.90 W/m^2.

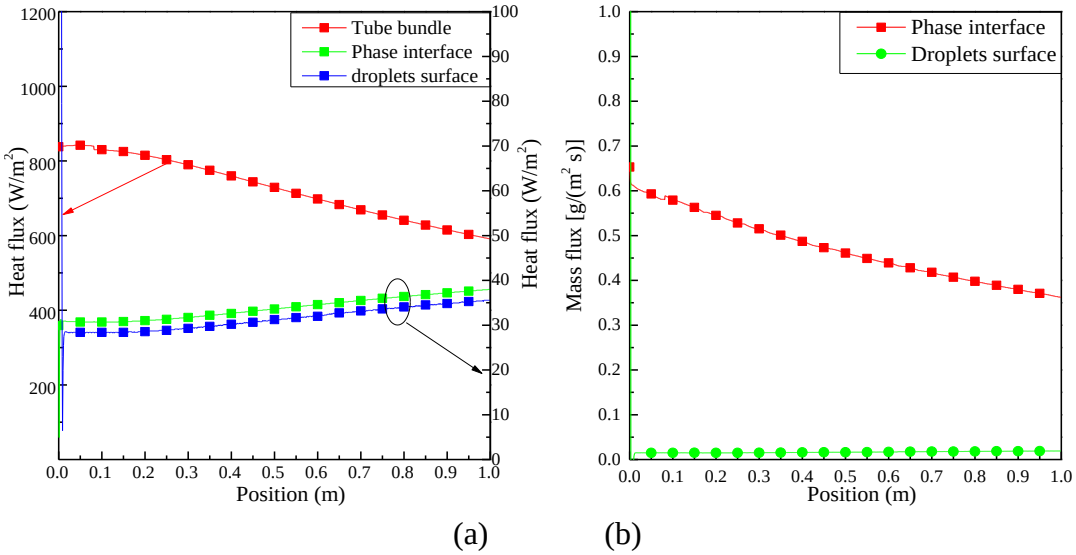

Fig. 6 The mass and heat transfer characteristics of Mode C

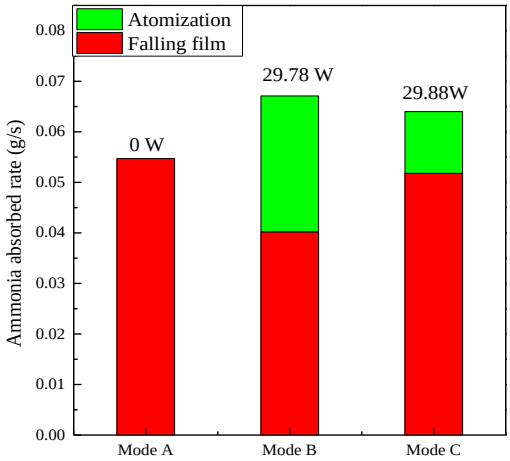

Fig. 7 The comparisons of ammonia absorbed rate of a falling film tube and the total atomization energy consumption of the absorber in different modes

In conclusion, compared with Mode A, the atomization lifts the vapor temperature, and Mode B has higher vapor temperature because of lower droplets mass fraction. Fig. 7 shows the comparison of ammonia absorbed rate of different Modes. Although the falling film absorption is weakened, more effective atomization absorption is utilized to obtain higher total ammonia absorbed effect of Mode B. Furthermore, the improvement of ammonia absorbed rate in Mode C is an extra increment based on the falling film absorption. However, in the operation condition listed in Table 2, since the higher ammonia mass fraction of droplets, the ammonia absorbed rate of atomization absorption process in Mode C is less than it in Mode B, which results that the overall enhancement of Mode C is worse than Mode B.

4.4. Further discussion

For the absorber, the ammonia absorbed rate of Mode A and Mode B and Mode C is 2.024 g/s and 2.479 g/s and 2.368 g/s, respectively. When the evaporation temperature is -15 ℃ and the condensation temperature is 30 ℃, if the superheat of the evaporator and the subcooling of condenser are neglected, the cooling capacity per weighting of ammonia is 1103 kJ/kg. With the mass flow rate of inlet solution listed in Table 2, the cooling capacity of evaporator is 2232 W, 2734 W and 2611 W in Mode A, Mode B and Mode C, respectively. Therefore, the energy consumption of about 30 W can increase the system cooling capacity by about 400 W, which means that the installation of the ultrasonic atomizer can increase the energy efficiency of the ARS.

Comprehensively, in the operation condition listed in Table 2, both Mode B and Mode C can increase the energy efficiency of the ARS by a little energy consumption. Moreover, Mode C can absorb more ammonia by increasing energy consumption, but the Mode B has an upper limit because its atomization ratio is smaller than 1. However, Mode B has better energy efficiency than Mode C.

5. Conclusion

A method of installing ultrasonic atomizer to enhance the ammonia absorption process of the falling film absorber is proposed in this paper. The enhancement effects of parallel (Mode B) and series (Mode C) installation strategies of the atomizer are considered, and the influence of the droplets parameter on the enhancement is also analyzed. The results indicate that: When the droplets diameter is 50 μm, both the installation strategies of ultrasonic atomizer can improve the ammonia absorbed rate of the falling film absorber, and the Mode B (in parallel) has better enhancement than Mode C (in series) at equal droplets mass flow rate. In the condition listed in Table 2, the improvement of ammonia absorbed rate in Mode B and Mode C is 22.5% and 17.0%, respectively.

Reference

[1] Xu X, Li Y, Yang S, Chen G. A review of fishing vessel refrigeration systems driven by exhaust heat from engines[J]. Applied Energy. 2017, 203: 657-676.

[2] Siddiqui M U, Said S A M. A review of solar powered absorption systems[J]. Renewable and Sustainable Energy Reviews. 2015, 42: 93-115.

[3] Xu Z Y, Wang R Z. Absorption refrigeration cycles: Categorized based on the cycle construction[J]. International Journal of Refrigeration. 2016, 62: 114-136.

[4] Abed A M, Alghoul M A, Sopian K, Majdi H, AI-Shamani A, Muftah A. Enhancement aspects of single stage absorption cooling cycle: A detailed review[J]. Renewable and Sustainable Energy Reviews. 2017, 77: 1010-1045.

[5] Boudéhenn F, Bonnot S, Demasles H, Lefranois F, Perier-Muzet M. Development and Performances Overview of Ammonia-water Absorption Chillers with Cooling Capacities from 5 to 100 kW[J]. Energy Procedia. 2016, 91: 707-716.

[6] Sun J, Fu L, Zhang S. A review of working fluids of absorption cycles[J]. Renewable and Sustainable Energy Reviews. 2012, 16(4): 1899-1906.

[7] Yuan H, Zhang J, Huang X, Mei N. Experimental investigation on binary ammonia – water and ternary ammonia – water – lithium bromide mixture-based absorption refrigeration systems for fishing ships[J]. Energy Conversion and Management. 2018, 166: 13-22.

[8] Aminyavari M, Aprile M, Pistocchini L, Motta M. Modelling and experimental validation of an in-tube vertical falling film absorber with counter flow arrangement of solution and gas[J]. International Journal of Refrigeration. 2019, 100: 72-82.

[9] Zhang X, Wu J, Li Z. Irreversibility characterization and analysis of coupled heat and mass transfer processes in an absorption system[J]. International Journal of Heat and Mass Transfer. 2019, 133: 1121-1133.

[10] Triché D, Bonnot S, Perier-Muzet M, Boudehenn F, Demasles H, Caney N. Experimental and numerical study of a falling film absorber in an ammonia-water absorption chiller[J]. International Journal of Heat and Mass Transfer. 2017, 111: 374-385.

[11] Amaris C, Bourouis M, Vallès M. Effect of advanced surfaces on the ammonia absorption process with NH3/LiNO3 in a tubular bubble absorber[J]. International Journal of Heat and Mass Transfer. 2014, 72: 544-552.
[12] Mao Y, Yu G. Absorption and Vapor Blasting Refrigerating Device (in Chinese)[M]. Beijing: China Machine Press, 1985.
[13] Yang Z, Zhang K, Yang M, Lian Z. Improvement of the ultrasonic atomization liquid desiccant dehumidification system[J]. Energy and Buildings. 2014, 85: 145-154.
[14] Jiang X, Siamas G A, Jagus K, Karayiannis T G. Physical modelling and advanced simulations of gas–liquid two-phase jet flows in atomization and sprays[J]. Progress in Energy and Combustion Science. 2010, 36(2): 131-167.
[15] Urbán A, Zaremba M, Malý M, Józsa V, Jedelsky J. Droplet dynamics and size characterization of high-velocity airblast atomization[J]. International Journal of Multiphase Flow. 2017, 95: 1-11.
[16] Ma S, Zang B, Song H, Chen G, Yang J. Research on mass transfer of CO2 absorption using ammonia solution in spray tower[J]. International Journal of Heat and Mass Transfer. 2013, 67: 696-703.
[17] Li Z, Ji X, Yang Z, Lu X. Experimental studies of air-blast atomization on the CO2 capture with aqueous alkali solutions[J]. Chinese Journal of Chemical Engineering. 2019, 27(10): 2390-2396.
[18] Bešenić T, Baleta J, Pachler K, Vujanović M. Numerical modelling of sulfur dioxide absorption for spray scrubbing[J]. Energy Conversion and Management. 2020, 217: 112762.
[19] Cui H, Li N, Peng J, Yin R, Li J, Wu Z. Investigation on the thermal performance of a novel spray tower with upward spraying and downward gas flow[J]. Applied Energy. 2018, 231: 12-21.
[20] Kuntz J, Aroonwilas A. Mass-transfer efficiency of a spray column for CO2 capture by MEA[J]. Energy Procedia. 2009, 1(1): 205-209.
[21] Kuntz J, Aroonwilas A. Performance of Spray Column for CO2 Capture Application[J]. Industrial & Engineering Chemistry Research. 2008, 47(1): 145-153.
[22] Sathish A, Sharma A, Gable P, Skiadas I, Brown R, Wen Z. A novel bulk-gas-to-atomized-liquid reactor for enhanced mass transfer efficiency and its application to syngas fermentation[J]. Chemical Engineering Journal. 2019, 370: 60-70.
[23] Zhang Y, Yuan S, Wang L. Investigation of capillary wave, cavitation and droplet diameter distribution during ultrasonic atomization[J]. Experimental Thermal and Fluid Science. 2021, 120: 110219.
[24] Kim K D, Jin D H, Choi Y C. Numerical simulation on the generation of ultrasound and formation of water fog in the ultrasonic gas atomizer[J]. Ultrasonics. 2020, 102: 105851.
[25] Yang Z, Zhang K, Hwang Y, Lian Z. Performance investigation on the ultrasonic atomization liquid desiccant regeneration system[J]. Applied Energy. 2016, 171: 12-25.
[26] Li W, Pan Y, Yao Y, Dong M. Modeling and parametric study of the ultrasonic atomization regeneration of desiccant solution[J]. International Journal of Heat and Mass Transfer. 2018, 127: 687-702.
[27] Aminyavari M, Aprile M, Toppi T, Garone S, Motta M. A detailed study on simultaneous heat and mass transfer in an in-tube vertical falling film absorber[J]. International Journal of Refrigeration. 2017, 80: 37-51.
[28] Jiang W, Li S, Yang L, Du K. Experimental investigation on enhancement of ammonia absorption process with TiO2 nanoparticles in newly designed absorber[J]. International Journal of Refrigeration. 2019, 100: 93-103.
[29] Xu Y, Chen X, Zhao Y, Jin B. Modeling and analysis of CO2 capture by aqueous ammonia+piperazine blended solution in a spray column[J]. Separation and Purification Technology. 2021, 267: 118655.
[30] Crowe C T, Schwarzkopf J D, Sommerfeld M, Tsuji Y. Multiphase Flows with Driolets and Particales(2nd Edition)[M]. New York: CRC Press, 2012.
[31] Incropera F P, Dewitt D P, Bergman T L. Fundamentals of heat and mass transfer[M]. 6 ed. Beijing: Chemical Industry Press, 2011.
[32] Gesellschaft V. VDI Heat Atlas[M]. Berlin: Springer Berlin Heidelberg, 2010.
[33] Avvaru B, Patil M N, Gogate P R, Pandit A B. Ultrasonic atomization: Effect of liquid phase properties[J]. Ultrasonics. 2006, 44(2): 146-158.